WELDING RESEARCH

SUPPLEMENT TO THE *WELDING JOURNAL*, OCTOBER 1996
Sponsored by the American Welding Society and the Welding Research Council

Shielding Gas and Heat Transfer Effeciency in Plasma Arc Welding

Shielding gas flow rate is shown to have an appreciable effect on the size of the weld and the HAZ

BY R. HOU, D. M. EVANS, J. C. McCLURE, A. C. NUNES AND G. GARCIA

ABSTRACT. Variable polarity plasma arc welding is widely used in the aerospace industry for producing high-quality welds on aluminum. In plasma welding the arc is produced in a narrow stream of plasma gas while workpiece shielding is accomplished by a lower velocity but higher flow rate stream of shielding gas that surrounds the arc. This paper will show that on aluminum welds both the melt zone and the heat-affected zone are appreciably decreased by this flow of shielding gas. Moreover, the amount of cooling is changed by the detailed shape of this flow as well as the flow rate. On the other hand, it will be shown that excessively high shielding flow rates can cause undercutting from contamination in the shielding gas.

Introduction

Variable polarity plasma arc welding (VPPA) has been used extensively by NASA and other demanding customers for high-quality welds on aluminum (Ref. 1). A schematic of the welding torch is shown in Fig. 1. The arc is carried by a constricted high-velocity stream of gas (usually argon) and weld pool shielding is accomplished by a concentric annular flow of helium. The high velocity plasma gas stream permits welding in the keyhole mode in which the arc penetrates through the workpiece (for example, a 300-A arc can easily produce a keyhole in 0.5-in. aluminum) to produce a stiff easily controlled arc and a clean porosity-free weld. The polarity of the welding electrode is changed (typically 19 ms DCEN and 3 ms DCEP) to produce cathodic cleaning of the refractory oxide on aluminum (Refs. 2–3).

The flow rate of the shielding gas is typically chosen (with a substantial safety margin) to prevent surface oxidation. The humidity of the environment and expected flow perturbations from the welding environment are considered in choosing an adequate flow rate. The shielding gas flows through an annular gas nozzle surrounding the arc and the shape of the shielding gas flow is determined by the configuration of the gas nozzle. It will be shown that heat is transferred to the shielding gas from the plasma gas and from the workpiece. This transfer of heat leads to a reduction in the fusion zone (FZ) and heat-affected zone (HAZ). Furthermore, a high flow rate of shielding gas can produce undercutting in a weld when low levels of contaminants are present in the gas. Even aside from the economic considerations of the cost of shielding gas, there appears to be an optimum shielding gas flow rate to produce good quality welds while guarding against contamination from the shielding gas. When comparing the properties of weldments made under similar conditions, attention must be paid to the shielding gas flow rate, as well as to the details of the shielding gas flow as determined by the torch and gas nozzle configuration.

Heat transfer during plasma welding has been studied by Metcalfe and Quigley, who calculated efficiencies of heat transfer to the anode for both keyhole (fully penetrated) and cover pass (unpenetrated) welds (Ref. 4). Fuerschbach (Ref. 5) has performed a careful study of both arc efficiency (total heat transferred to the workpiece/weld power) and melting efficiency of both plasma arc welding (PAW) and gas tungsten arc welding (GTAW). In neither case, however, was the cooling effect of the

KEY WORDS

Plasma Arc Welding
Shielding Gas
Heat Transfer
Melt Efficiency
Undercutting
HAZ
Al 6016
VPPA

R. HOU, D. M. EVANS, and J. C. McCLURE are with the Metallurgical and Materials Engineering Department, University of Texas at El Paso, Tex. A. C. NUNES is with NASA Marshall Space Flight Center, Huntsville, Ala. G. GARCIA is with the Institute of Metallurgy, University of San Luis Potosi, San Luis, Mexico.

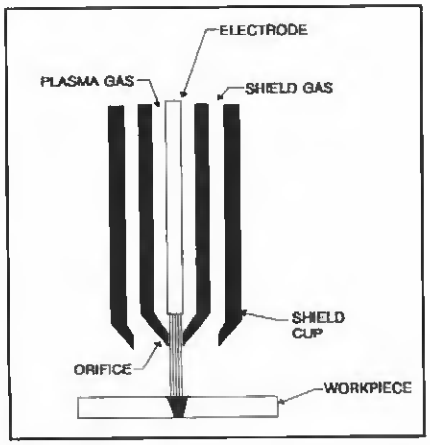

Fig. 1 — Schematic of VPPA welding torch.

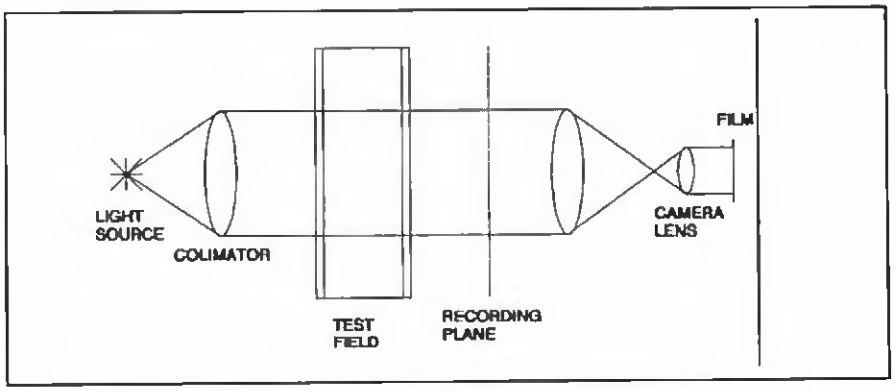

Fig. 2 — Shadowgraph system for visualizing the flow patterns in VPPA welding.

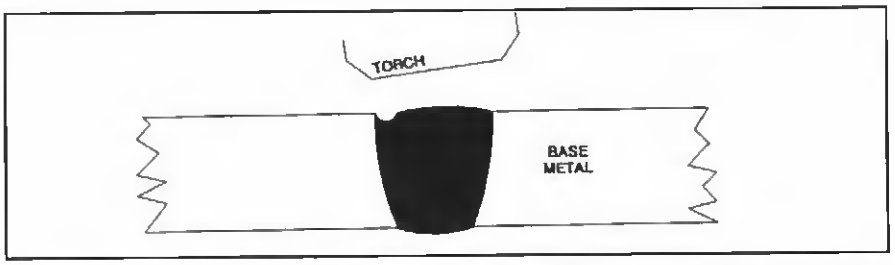

Fig. 3 — Schematic of weld torch, workpiece and undercutting. Note how the tilted torch causes undercutting on the upper left corner of the weld bead.

Table 1 — Parameters for Equation 1 (Refs. 8, 9)

Cp	5.19×10^3 J/kg·K (at 25°C)
μ	1.968×10^{-5} N·s/m² (at 25°C)
κ	0.151 W/m·K (at 25°C)
ρ	0.1604 Kg/m³
V∞	1.14 m/s
Pr	0.676
Re	96
X/S	5
H/S	1.75
m	0.597
Nu	2.432

Table 2 — Characteristics of Gas Nozzles

Gas Nozzle	Area (cm²) Length (cm) Comments
1 (R) 2.774.75	Standard nozzle
2 (SR) 2.074.90	Reduced area and 1.5 mm longer
3 (R') 2.774.90	Standard nozzle but 1.5 mm longer

Table 3 — Welding Conditions

Gas Nozzle	Voltage (V)	Current (A)	Shielding Flow Rate Range
1 (R)	30	120	27.5–50 ft³/h
2 (SR)	30	120	15–40 ft³/h
3 (R')	30	120	20–40 ft³/h

shielding gas addressed.

The amount of heat put into the workpiece changes due to heat transfer from the arc to shielding gas. Also, the melting efficiency, which is the amount of heat needed to create the observed fusion zone divided by the net heat input to the workpiece, may vary due to heat transfer from the workpiece to the shielding gas. The effect of impingement cooling of the workpiece by the stream of shielding gas can be estimated from Equation 1, which is for a single slot nozzle (Ref. 6).

Where Nu = Nusselt number = hS/k

Pr = Prandtl number = μCp/k

$$\frac{Nu}{Pr^{0.42}} = \frac{1.53}{X/S + H/S + 1.39} Re^{m(X/S, H/S)}$$

$$m = 0.695 - \left[X/S + (H/S)^{1.33} + 3.06 \right]^{-1} \quad (1)$$

Where Re = Reynolds number = SV_∞/γ; h = heat transfer coefficient; S = characteristic length = 2 X width of slot; k = thermal conductivity of gas; μ = viscosity; Cp = specific heat capacity of the gas; V_∞ = velocity of gas; γ = kinematic viscosity = μ/ρ; H = distance between the nozzle and solid surface; X = half of the surface width covered by the impinging gas.

For typical VPPA welding conditions, the parameters appearing in this equation, as well as the calculated results, are listed in Table 1. The S dimension was 4 mm, H was 7 mm, and X was 20 mm. When the shielding gas exits from the shielding gas nozzle and hits the workpiece, a wall jet is produced. According to wall jet theory (Ref. 7), the velocity of a wall jet is reduced to about 90% of the outlet velocity from the slot within a 2 cm range.

From Nu, the heat loss due to convective heat transfer between the shieldinging gas and workpiece can be estimated and a value of 149 J/s was obtained. Since typical welding voltage and current are 30 V and 120 A, respectively, and arc efficiency (heat transferred to workpiece/total energy input) is approximately 55% (Refs. 4, 5), the convective heat loss represents about 7.5% of the total energy input to the workpiece. Note that the measured melting efficiency of these welds is only about 7.6% for the slow welding speed of 4 mm/s that was used.

In addition, this cooling is greatest at the edge of the weld pool where the stream of shielding gas turns from perpendicular to parallel to the workpiece. It is here that the largest microstructural effect of the impingement cooling would be expected.

Table 4 — Welding Conditions for Undercut Tests

Voltage (V)	Current (A)	Torch Tilt Angle	Shielding Gas	Shielding Flow Rate
30	150	3	clean helium	20–40 ft³/h
30	150	4	clean helium	20–40 ft³/h
30	150	4	N_2 contaminated	20–40 ft³/h
30	150	0	CH_4 contaminated	20 & 40 ft³/h

Experimental Details

All welds were made with a Hobart variable polarity 300 series power supply and control console. A carefully aligned Buggo torch tractor was used for all welds. The standard welding torch and gas nozzle was supplied by B & B Co. The characteristics of the cups are shown in Table 2.

With the standard nozzle, the distance between the gas nozzle and the workpiece with a 30-V arc is 7 mm. Cups 2 and 3 are thus 21% closer.

A shadowgraph system to visualize the flow patterns in VPPA welding was set up and mounted to the welding system. This shadowgraph system is shown in Fig. 2 and details can be found in Ref. 10.

Aluminum 6061 plates with a thickness of 6.2 mm (0.25 in.) were used in the experiments. They were degreased and etched prior to welding. The welding conditions are listed in Table 3. All welds were uphill bead-on-plate and made at 4.1 mm/s.

Samples were sectioned from each weldment, mounted, ground, and polished to 1 μm with alumina powder and etched with Keller's Reagent. Finally, the cross section of each sample was observed and measured optically and the heat-affected zone (HAZ) width was determined by a Vicker's microhardness traverse 0.5 mm below the surface of the weld. The aspect ratio, which is the ratio of half the weld width to the weld depth,

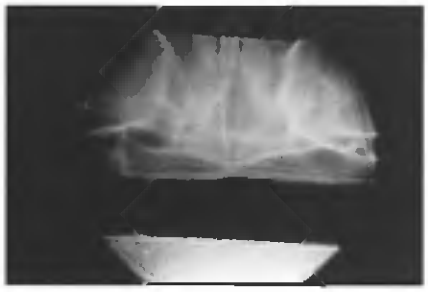

Fig. 4 — Shadow graph of the plasma arc. The torch is at the top of the picture. Both plasma and shielding gas flows can be seen. The standoff distance is approximately 13 mm.

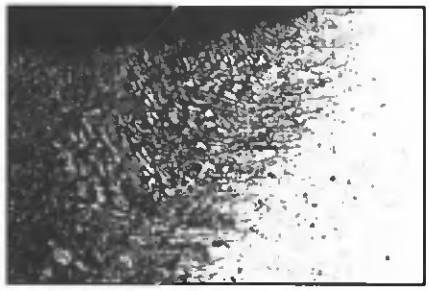

Fig. 5 — Cross section of a weld. From left to right are the molten zone, optically observable portion of the heat-affected zone and the base metal.

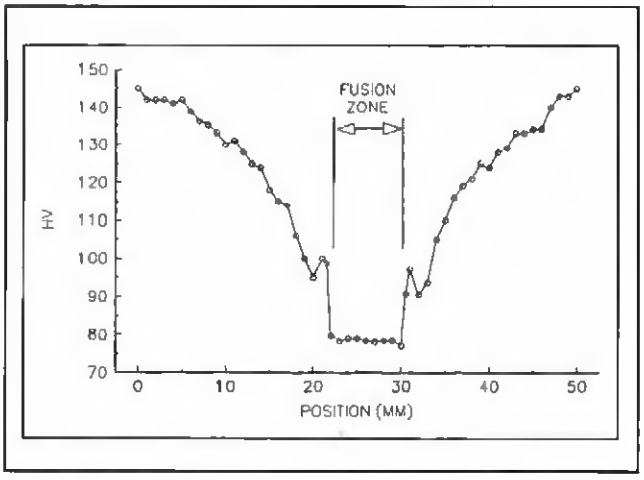

Fig. 6 — Typical microhardness traverse used to determine the heat-affected zone width.

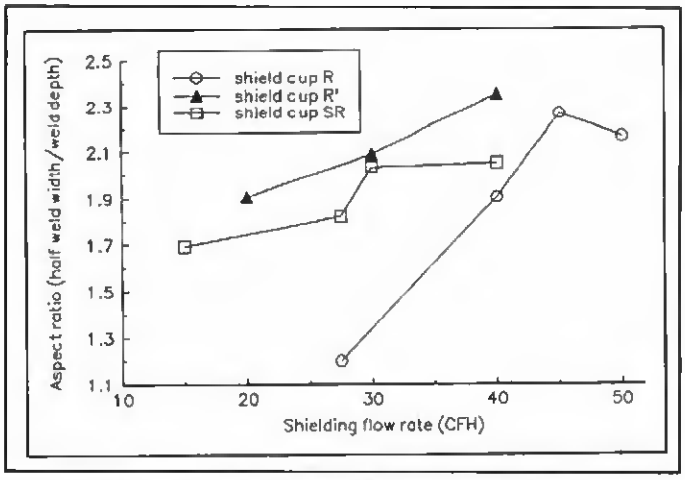

Fig. 7 — Aspect ratio vs. shielding gas flow rate. The weld with a standard torch (R) and 27.5 ft³ of shielding gas shows an unacceptable oxidized surface.

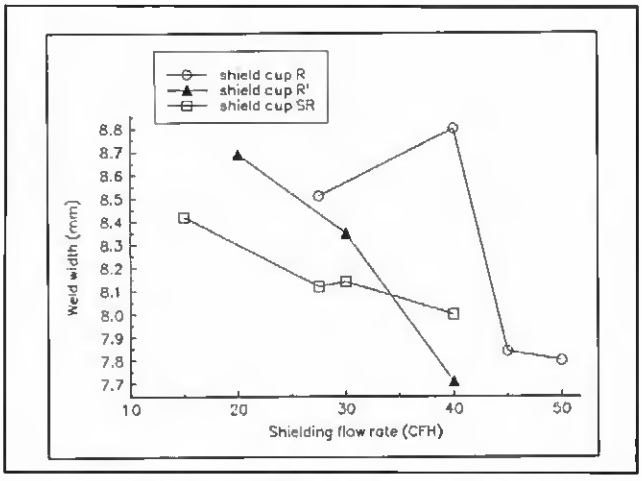

Fig. 8 — Weld width vs. shielding gas flow rate. The weld with the standard cup (R) and 2.75 ft³ of shielding gas shows unacceptable surface oxidation.

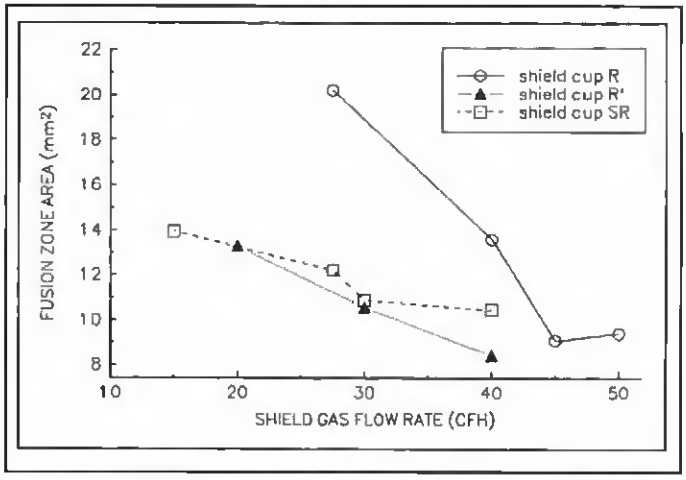

Fig. 9 — Fusion zone area vs. shielding gas flow rate.

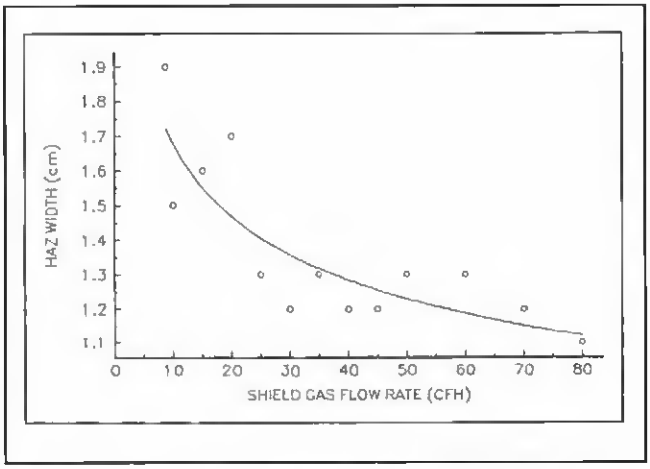

Fig. 10 — Heat-affected zone width vs. shielding gas flow rate.

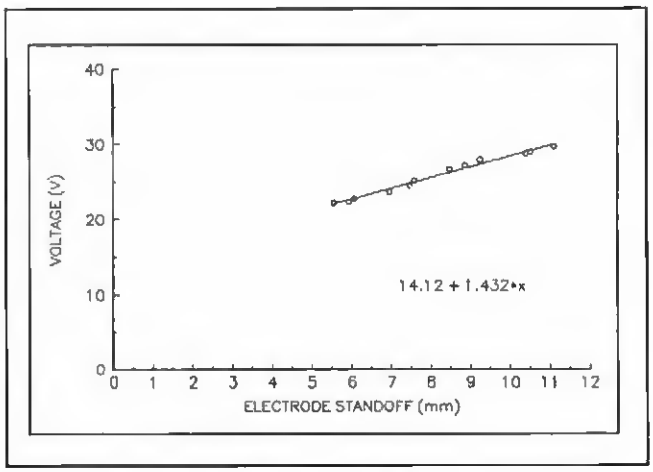

Fig. 11 — Voltage vs. electrode standoff distance.

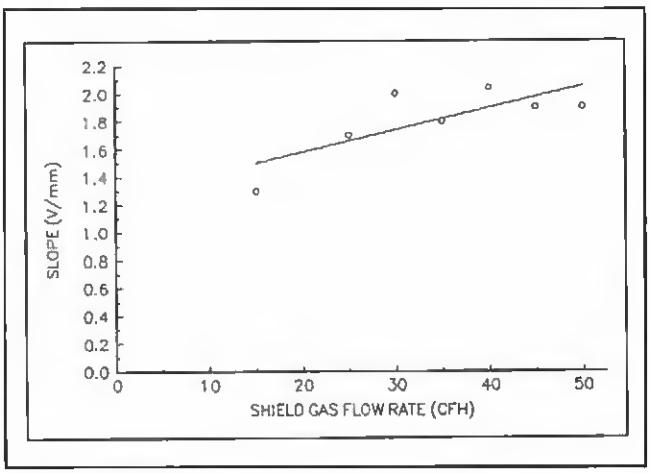

Fig. 12 — Slope of voltage vs. standoff plots for various shielding gas flow rates. Note that slope is proportional to arc resistance.

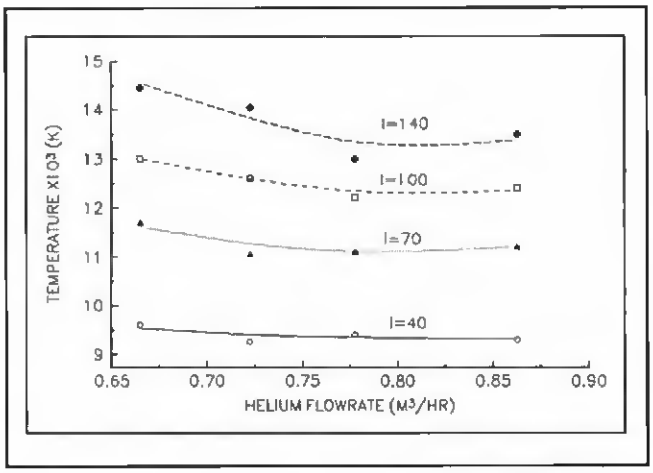

Fig. 13 — Average arc temperature vs. shielding gas flow rate for various welding currents. Temperature measured spectroscopically.

and the fusion zone (FZ), which was calculated as 2/3 the weld depth times width (Ref. 11), were measured.

To study the effects of torch alignment and shielding gas on undercutting, an apparatus was designed in which the torch was rigidly mounted to a large protractor and held stationary while the workpiece was moved downward. This permitted measurement and control of the torch tilt angle in a plane perpendicular to the workpiece and the torch travel direction. Undercutting was observed on the same side of the torch as the tilt as shown in Fig. 3. The amount of undercut was measured as the depth of the groove as shown in this figure.

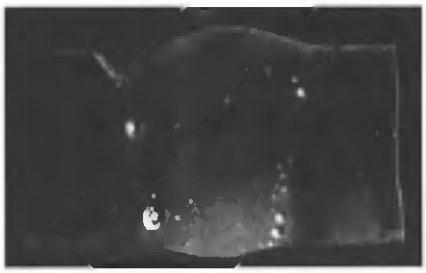

Fig. 14 — Cross section of a weld made with a 500 ppm CH_4 contaminated shielding gas and 40 ft³/h shielding gas flow rate. Undercutting is seen on the left side. Note the unacceptable porosity in the weld.

Welds were also made on Al 6061 for the undercutting test. Only the standard gas nozzle was used at this time. The welding conditions are listed in Table 4.

Results and Discussion

Figure 4 shows a shadowgraph of the gas flow with typical shielding and plasma gas flow rates. To avoid the difficulties of index of refraction changes due to electron density (Ref.10), the welding arc was not turned on and only the pilot arc was used. Note that the central plasma column is well confined and that the shielding gas strikes the workpiece and eventually becomes turbulent away from the center of the torch.

Figure 5 shows a typical weld cross-section. The melt zone, heat-affected zone and base metal can be seen. The heat-affected zone width is determined by microhardness testing. A typical hardness traverse is shown in Fig. 6. The flat portion of Fig. 6 corresponds to the fusion zone, and it is seen that the hardness increases in the heat-affected zone until it reaches the hardness of the base metal. The aspect ratio and weld width for different weld samples with various shielding flow rates and gas nozzles are shown in Figs. 7 and 8. The FZ and HAZ width for all samples are shown in Figs. 9 and 10.

The length of the gas nozzle affects the minimum shielding flow rate needed for protection from the atmosphere. With the standard gas nozzle, the welds become oxidized and unacceptable when a shielding flow rate less than 19 L/min (40 ft³/h) is used. In contrast, even when the flow rate is reduced to 9.4 L/min (20 ft³/h), the welds with the longer gas nozzles (R′ and SR) produced smooth and

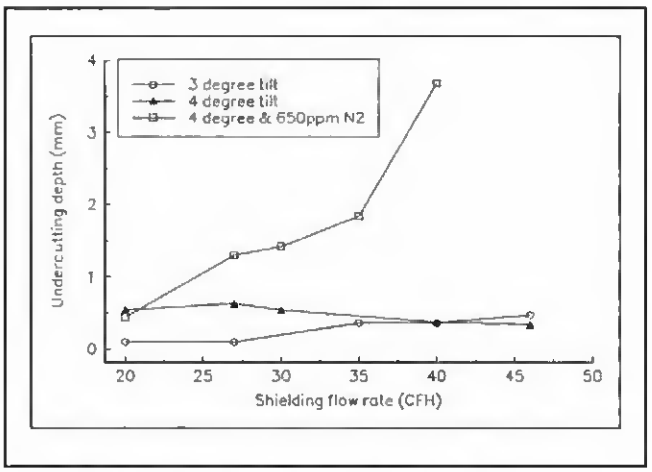

Fig. 15 — Undercutting vs. shielding gas flow rate.

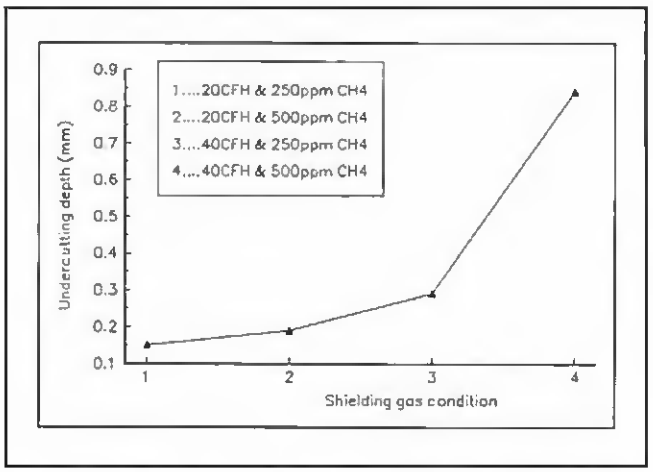

Fig. 16 — Undercutting vs. shielding gas contamination. Note how undercutting increases with increase in volume of shielding gas.

shiny surfaces with no porosity, indicating adequate shielding. The reduced length of the shielding gas column with these nozzles means that less shielding gas is needed to keep out atmospheric contamination.

It is seen that the weld aspect ratio increases, while FZ and HAZ width are decreased with an increase in shielding gas flow rate. These changes occur with all three gas nozzles.

A lower shielding gas flow rate will result in a smaller shielding gas velocity and a smaller Reynolds number. This reduces the heat loss due to convective heat transfer between the shielding gas and workpiece. From Equation 1, it is seen that heat transfer is proportional to $Re^{0.597}$. If the flow rate is reduced by half, both velocity and Re are reduced by half and the heat loss due to this impinging shielding gas will be approximately 30% less. The mechanical properties of welds made with differing FZs and HAZs are expected to differ and are presently being studied.

There is some evidence to support the theory that the shielding gas cools the arc as well. A series of graphs was made of voltage vs. electrode standoff for various shielding gas flow rates (Fig. 11 shows a typical graph). The slope represents the resistance of the arc. The steeper the slope the higher the resistance. As shown in Fig. 12, the slope increases as the shielding gas flow rate increases, indicating that the arc resistance is increasing. The resistance of plasma is proportional to $T^{3/2}$, where T = temperature (Ref. 12). Therefore, the temperature of the arc decreases as the shielding gas flow rate increases. Data in Fig. 13 show results of spectroscopic measurements by Pang indicating a cooler arc with the increased shielding gas flow rate (Ref. 13).

The configuration of the gas nozzle also affects the convective heat transfer as seen in Fig. 9. The longer nozzles, R' and SR, have a shorter distance to the workpiece and H in Equation 1 is reduced. At the same flow rate, Nu increases and the final heat transfer increases.

Of the two nozzles with the same length, it was anticipated that the nozzle with the smaller exit area, SR, would further increase the heat transfer. Figure 9, however, shows little difference between R' and SR. Perhaps, the relevant characteristic length in calculating the Reynold's number is the internal "throat velocity" (or velocity at smallest cross section) of the nozzle, which is the same for both nozzles. In any case, a heat flow calculation in this complicated situation would be highly empirical.

Figure 14 is a cross section of a weld sample made with a tilted torch and contaminated shielding gas. Undercutting on the left side, which is the side away from the torch tilt, is apparent. The undercutting as a function of shielding gas flow rate and shielding gas contamination is shown in Figs. 15 and 16. In Fig. 15, the welds were made with a tilted welding torch and commercially pure helium or helium contaminated with nitrogen using various flow rates. Although undercutting was present with pure gas, the undercutting did not change appreciably with flow rate. The contaminated gas undercutting, however, increased nearly sevenfold as flow rate was increased. Thus, undercutting can be caused by both atmospheric contamination from a tilted torch and from shielding gas contamination at large shielding gas flow rates. In Fig. 16, welds were made with a nontilted torch but a highly contaminated shieldinging gas. Undercutting increases with the total amount of contamination input to the weld pool. It does not matter whether this input originates from more highly contaminated gas or from a higher flow rate.

It is believed that this undercutting results from either atmospheric or shielding gas contamination on the less well shielded side of the arc. Such contamination will change the gradient of surface tension and cause asymmetry of Marangoni flow on the weld pool and cause the observed undercutting.

Conclusions

1) The size of the fusion zone and heat-affected zone is decreased by increasing the shielding gas flow rate in plasma arc welding. It is proposed that these changes are due to convective heat transfer between the impinging shielding gas and solid workpiece and by heat transfer between the arc and the shielding gas.

2) Undercutting is affected by the shielding gas in plasma arc welding. In general, undercutting becomes worse with an increase of flow rate and gas contamination because of an increase of gas contamination input to the weld pool. This is ultimately caused by the asymmetric surface tension gradient in the weld pool.

Acknowledgment

The generous support of NASA Marshall Space Flight Center under contract number NAS8-39602 is gratefully acknowledged.

References

1. Nunes, A. C., *et al.* 1984. Variable po-

larity plasma arc welding on the space shuttle external tank. *Welding Journal* 36(9): 15–25.

2. Lancaster, J. F. 1984. *Physics of Welding*. p. 116, Pergamon Press, New York, N.Y.

3. Pang, Q., Pang, T., McClure, J.C., and Nunes, A. C. 1994. Workpiece cleaning during variable polarity plasma arc welding of aluminum. *Journal of Engineering for Industry* 116(4): 463–466.

4. Metcalfe, J. C., and Quigley, M. B. C. 1975. Heat transfer in plasma arc welding. *Welding Journal* 27(3): 99-s to 103-s.

5. Fuerschbach, P. W., and Knorovsky, G. A. 1991. A study of melting efficiency in plasma arc and gas tungsten arc welding. *Welding Journal* 43(11): 287-s to 297-s.

6. Vargaftok, N. B. 1975. *Tables on the Thermophysical Properties of Liquids and Gases*. New York, N.Y., John Wiley & Sons, Inc.

7. Davies, J. T. 1972. *Turbulence Phenomena*. p. 152, New York, N.Y., Academic Press.

8. Pankratz, L. B. 1982. *Thermodynamic Properties of Elements and Oxides*. p. 185, Washington, D.C., United States Department of the Interior.

9. Martin, H. 1977. Heat and mass transfer between impinging gas jets and solid surfaces. *Advances in Heat Transfer*, Vol. 13, pp. 1–26.

10. Hou, R. 1994. Study of gas flow pattern, undercutting and modification of welding torch in variable polarity plasma arc welding. pp. 12–43, M.S. thesis, The University of Texas at El Paso, El Paso, Tex.

11. Liu, J. T., Weckman, D. C., and Kerr, H. W. 1993. The effects of process variables on pulsed Nd:YAG laser spot welds — part I AISI 409 stainless steel. *Metall. Trans.* 24B (6): pp. 1065–1076.

12. Chen, F. F. 1984. *Introduction to Plasma Physics and Controlled Fusion*, Vol. 1. pp. 178–183. Plenum Press, New York, N.Y.

13. Pang, Q. 1991. In situ spectroscopic measurements of variable polarity plasma arc welding of aluminum 2219. p. 90. M.S. Thesis, the University of Texas at El Paso, El Paso, Tex.